Controlled Hydrolysis of Phosphate Esters: A Route to Calixarene-Supported Rare-Earth Clusters

Marjan Hosseinzadeh,*[a] Sergio Sanz,*[b] Jan van Leusen,[a] Natalya V. Izarova,[a] Euan K. Brechin,*[c] Scott J. Dalgarno,*[d] and Paul Kögerler*[a, b]

Abstract: Phosphate ester bonds are widely present in nature (e.g. DNA/RNA) and can be extremely stable against hydrolysis without the help of catalysts. Previously, we showed how the combination of phosphoryl and calix[4]arene moieties in the same organic framework (L_{PO}) allows isolation of single lanthanide (Ln) metal ions as $[Ln^{III}(L_{PO})_2](O_3SCF_3)_3$. Here we report how by controlling the reaction conditions a new hydrolyzed phosphoryl-calix[4]arene ligand (H_3L_{HPO}) is formed as a result of Ln^{III}-mediated P–OEt bond cleavage in three out of the eight possible sites in L_{PO}. The chelating nature of H_3L_{HPO} traps the Ln^{III} species in the form of $[Ln^{III}(L_{HPO})((EtO)_2P(O)OH)]_2$ dimers (Ln = La, Dy, Tb, Gd), where the Dy derivative shows slow magnetization relaxation. The strategy presented herein could be extended to access a broader library of hydrolyzed platforms (H_xL_{HPO}; $x = 1–8$) that may represent mimics of nuclease enzymes.

Introduction

The bowl-shaped *p-tert*-butylcalix[4]arene (TBC[4]) is a readily accessible, versatile supramolecular platform for metal complexation in the design of molecules with interesting physical characteristics, including single-molecule magnets (SMMs).[1] Compounds of *f*-elements play a prominent role in this regard given their large intrinsic magnetic anisotropy and have been suggested for potential application in quantum computation and molecular spintronics.[2] The four phenolic O atoms at what is termed the lower-rim render it an excellent candidate for the design of polynuclear complexes containing Ln^{III} ions.[3] The synthesis of calix[n]arene-supported mononuclear complexes of Ln^{III} centers has received less attention and typically requires the alkylation of the phenolic groups to limit the bridging nature of the ligand. Indeed, only three monometallic molecules have been reported as SMMs with TBC[4], one of which is a seven-coordinate Dy ion encapsulated between a TBC[4] and a Kläui-type tripodal ligand.[4]

In 2021, motivated by the success of the Kläui tripodal ligand[5] in coordinating Ln ions (132 complexes in the Cambridge Structural Database) via a facial κ^3-moiety (P=O), we retrieved an old synthetic protocol in which the TBC[4] ligand was converted into a tetradentate κ^4-TBC[4] unit to coordinate to a La ion for metal extraction.[6] This ligand allowed us to obtain the paramagnetic analogs with Tb^{III} and Dy^{III}, with the latter displaying slow relaxation of the magnetization.[4b] Here, the Dy^{III} ion is encapsulated between two tetrakis-*O*-(diethoxyphosphoryl)-*p-tert*-butylcalix[4]arene (L_{PO}) ligands and is eight-coordinate in a square-antiprismatic O_8 environment, $[Dy^{III}(L_{PO})_2](O_3SCF_3)_3$. These are the only three structures reported with this ligand; all synthesized in dry solvents. Indeed, phosphate ester bonds present remarkable kinetics and can only be hydrolyzed under specific conditions.[7] The hydrolysis of phosphate ester bonds, which are widely present in living systems, is an important biochemical reaction[8] and plays a fundamental role in DNA repair,[9] energy transduction,[10] and biomass conversion.[11] The majority of enzymes with the ability to catalyze hydrolysis reactions contain two or more metal ions in their active site.[12] Knowing the critical role of metal centers in these enzymes, artificial enzymes were developed – including luminescent lanthanide compounds – to gain a molecular-level understanding of their mechanism.[13] Inspired by this phenomenon, we report the controlled hydrolysis of the P–OEt bonds that transform the L_{PO} ligand into the new hydrolyzed version H_3L_{HPO}.

[a] Dr. M. Hosseinzadeh, Dr. J. van Leusen, Dr. N. V. Izarova, Prof. P. Kögerler
Institute of Inorganic Chemistry
RWTH Aachen University
52056 Aachen (Germany)
E-mail: marjan.hosseinzadeh@ac.rwth-aachen.de
paul.koegerler@ac.rwth-aachen.de

[b] Dr. S. Sanz, Prof. P. Kögerler
Peter Grünberg Institute,
Electronic Properties (PGI-6) Forschungszentrum Jülich
52425 Jülich (Germany)
E-mail: s.calvo@fz-juelich.de

[c] Prof. E. K. Brechin
EaStCHEM School of Chemistry
The University of Edinburgh
EH9 3FJ Edinburgh (UK)
E-mail: ebrechin@ed.ac.uk

[d] Dr. S. J. Dalgarno
Institute of Chemical Sciences
Heriot-Watt University
EH14 4AS Edinburgh (UK)
E-mail: S.J.Dalgarno@hw.ac.uk

Chemistry–A European Journal

Research Article
doi.org/10.1002/chem.202203525

Chemistry Europe
European Chemical
Societies Publishing

Results and Discussion

Synthesis and structural details

H_3L_{HPO} stems from a hydrolysis reaction in the L_{PO} ligand mediated by Ln^{III} metal ions acting as Lewis acids. Three (out of eight) P–OEt bonds are hydrolyzed, which belong to three different phosphate ester groups of the H_3L_{HPO} ligand (P2, P3, and P4 in Figure 1d). The chelating nature of the H_3L_{HPO} unit locks the two Ln^{III} ions into the stable dimer complexes $[Ln^{III}(L_{HPO})((EtO)_2P(O)OH)]_2$, (Ln = La (**1**), Dy (**2**), Tb (**3**), Gd (**4**)). Complete hydrolysis of the L_{PO} ligand would entail cleavage of eight P–OEt bonds per calixarene unit and the formation of H_8L_{HPO}.

Complexes **1**–**4** were synthesized by reacting L_{PO}, lanthanide trichloride and sodium diethyl phosphate (in a 1:1:3 ratio) in wet acetonitrile for two hours. After filtration, diethyl ether was diffused into the mother liquor of each complex, affording colorless crystals of **1**–**4** in high yields (~70%) after two weeks. They crystallize in a triclinic system and in each case structure solution was performed in the space group P-1. The asymmetric unit, in all four structures, comprises half of the molecule. Unit cell measurements confirm that compounds **1**–**4** are structurally analogous (see Experimental section and Table S1 in Supporting Information), hence structure **1** will be discussed in detail as a representative example (Figure 1c). $[L_{HPO}]^{3-}$ adopts a cone conformation and binds to the two La^{III} ions as hexadentate ligand through the oxygen atoms of the lower four phosphoryl groups: O11 ($O11\cdots La1$: 2.531(4)) Å, O21 ($O21\cdots La1$: 2.421(3) Å), μ_2-O31 ($O31\cdots La1$: 2.463(3) and $O31\cdots La1'$: 2.735(3)), O32 ($O32\cdots La1'$: 2.583(3) Å), O42 ($O42\cdots La1'$: 2.452(4)) and O41 ($O41\cdots La1$: 2.471(3) Å). The same distances are found in the other $[L_{HPO}]^{3-}$ unit due to the inversion center in the middle of the molecule (highlighted as a yellow dot in Figure 1c). The

coordination around La^{III} ions is best described as bicapped trigonal prismatic with the remaining coordination site occupied by the terminally bonded diethyl hydrogen phosphate ($La1\cdots O51$: 2.452(4) Å). The core of **1** thus consists of a $[La1-(\mu_2-O31)_2-La1']$ skeleton (La$\cdots$La: 4.295(1) Å, La–O–La angle: 111.3(1)°). In the crystal lattice, the molecules are interdigitated and pack in a parallel array. There is an intramolecular hydrogen bond between $O52((EtO)_2P(O)OH)-O23(phosphoryl_{calixarene})$ at 2.418(6) Å with the shortest intermolecular contact between adjacent molecules mediated by $O53((EtO)_2P(O)OH)-C210(tert-Butyl)$ interactions at 3.53(1) Å (Figure S1, see Supporting Information).

Upon changing reaction conditions in the synthesis of **1**–**4** by a) increasing the amount of $Ln^{III}Cl_3$ in the reaction, b) doubling the amount of sodium diethyl phosphate, c) adding more water by using hydrated precursors $Ln^{III}Cl_3\cdot6H_2O$, d) changing the solvent to a DMF/CH_3CN or DMF/EtOH mix (1/1, v/v) and e) introducing imidazole as co-ligand, no further hydrolysis reaction to the H_3L_{HPO} ligand was observed. The only structural change came from the added extra reactants (from sections c–d; H_2O, DMF and imidazole, respectively) affording the complexes $[Ln^{III}(L_{HPO})(X)]_2$ (Ln = Dy, X = H_2O (**5**); Ln = Dy, X = DMF/H_2O (**6**); Ln = Tb, X = DMF (**7**); Ln = Tb, X = imidazole (**8**)). Complexes **5**–**8** are structurally similar to **1**–**4**, only differing in their terminally bonded ligands at the Ln^{III} ions. Details of the synthesis of **5**–**8** and SCXRD data and discussions are given in the Supporting Information. Due to the structural similarity, complexes **5**–**8** were not further studied.
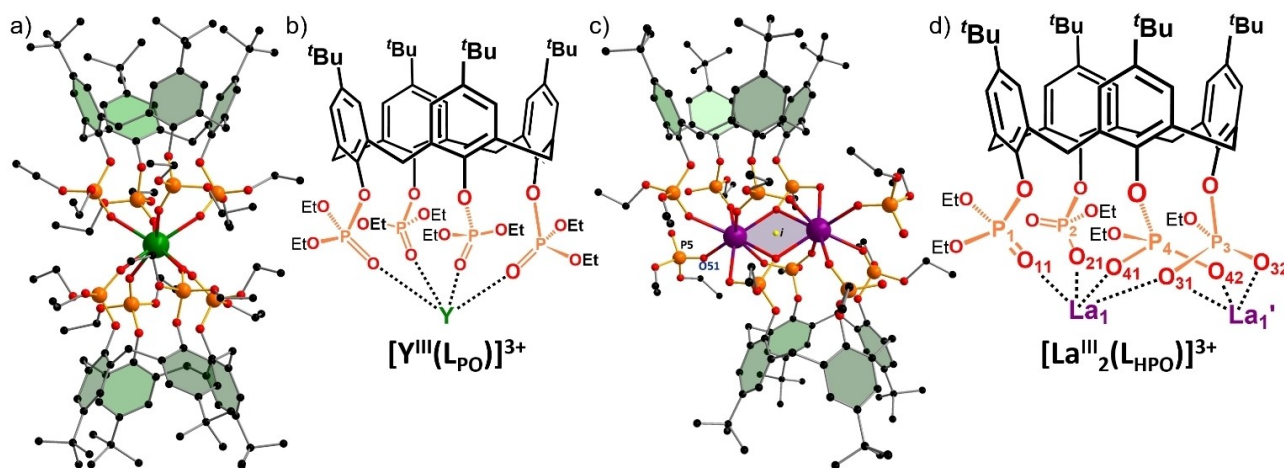

Figure 1. a) Molecular structure of $[Y^{III}(L_{PO})_2]^{3+}$ where L_{PO} acts as a tetradentate κ^4-ligand (P=O) to coordinate to a single Y^{III} ion. b) ChemDraw representation of the $[Y^{III}(L_{PO})]^{3+}$ fragment. c) Structure of the neutral $[La^{III}(L_{HPO})((EtO)_2P(O)OH)]_2$ molecule **1** where the hexadentate $[L_{HPO}]^{3-}$ ligand stems from the hydrolysis in the $(EtO)_2P=O$ groups of the neutral L_{PO}. Both La^{III} atoms (La1 and La1' in Figure 1d) are symmetry equivalent via inversion center i, shown as a yellow dot in the center of the purple plane containing both ions. d) ChemDraw representation of the $[La^{III}_2(L_{HPO})]^{3+}$ fragment depicting the binding modes of the $[L_{HPO}]^{3-}$ ligand coordinating to the La^{III} ions. Color code: Y: green, La: purple, O: red, P: orange, C: black, C–C/C–O bonds: gray, P–O bonds: orange, coordinative bonds: two-colored. H atoms, co-crystallized acetonitrile molecules and OTf⁻ anions in (c) are omitted for clarity.

Chemistry–A European Journal

Research Article
doi.org/10.1002/chem.202203525

Chemistry Europe
European Chemical
Societies Publishing

Analytical characterization

NMR experiments

We performed one-dimensional (1D) and two-dimensional (2D) NMR experiments in $CDCl_3$ for full characterization of the diamagnetic analog **1** in solution. The ^{31}P NMR (162 MHz, $CDCl_3$) of **1** exhibits five singlets at −5.62, −8.46, −9.02, −10.44 and −11.50 ppm corresponding to five structurally inequivalent phosphorus environments of the phosphoryl groups (L_{PO} shows a unique signal at −4.54 ppm) (Figure S2). The ^1H NMR (400 MHz, $CDCl_3$) spectrum shows one triplet at 0.85 ppm and a multiplet between 1.25–1.37 ppm related to the seven methyl groups ($POCH_2CH_3$) in the phosphoryl units in $[L_{HPO}]^{3-}$ and the one terminally bonded to La. The four singlets of the *tert*-butyl groups of the calixarene ligand are located at 1.14, 1.17, 1.19 and 1.23 ppm.

The methylene ($POCH_2CH_3$) protons split into two multiplets, at 3.01 and 3.68–4.74 ppm, related to the phosphoryl groups belonging to the calixarene and terminally bonded $(EtO)_2P$-(O)OH units (Figure 2b). The *axial* protons of the diastereotopic methylene bridges present four sets of doublets at 4.93, 5.19, 5.28 and 5.71 ppm, whereas, the *equatorial* protons are less affected by the complex formation exhibiting more localized signals in the frequency range 3.22–3.33 ppm (L_{PO} displays only doublets at $CH_{2eq} = 3.27$ and $CH_{2ax} = 4.80$ ppm). We performed Total Correlation Spectroscopy (TOCSY) to correlate *equatorial* and *axial* coupled protons in the calixarene unit (Figure S3). The

low symmetry in the molecule is also observed in the aromatic protons with eight sets of singlets between 6.99 and 7.13 ppm (symmetry equivalent H_{aro} in L_{PO} shows only one singlet at 6.88 ppm). The phosphoryl methylene protons are the most affected upon coordination to the lanthanide centers and to achieve an accurate recognition of each proton and the phosphoryl group to which they belong we performed 2D experiments – Homonuclear Correlation Spectroscopy (COSY) and ^1H-^{31}P Heteronuclear Multiple Bond Correlation (HMBC). From this information (see COSY in Figures S4–S7), we can confirm that the phosphorous signal at −5.62 ppm comes from a single chemical environment and corresponds to the terminally bonded diethyl hydrogen phosphate unit containing P5 (Figure 2b) whose four methylene protons resonate at 4.09 ppm in the ^1H NMR. The unhydrolyzed diethoxyphosphoryl unit (P1) presents a phosphorous signal at −10.44 ppm, correlating with four methylene protons at 4.74 and 4.46–4.37 ppm and, six methyl protons at 1.35 ppm by HMBC. Among the remaining (hydrolyzed) phosphoryl units, the one terminally coordinated to the lanthanide (P2; ^{31}P: $\delta = -11.50$ ppm) is the most shielded as can be seen by ^1H NMR in δ_{CH2} and δ_{CH3}. Identification of the remaining bridging phosphoryl units is more complicated; we speculate that the P3-phosphoryl unit with bridging modes μ_2-$\eta^2(O31)$:$\eta^1(O32)$ (Figure 1d) should be more deshielded and therefore show higher chemical shifts in ^1H NMR. Hence, these may correspond to the phosphorous signal at −8.46 ppm. The last phosphoryl unit (P4) binding to the Ln ions as μ_2-$\eta^1(O41)$:$\eta^1(O42)$ should
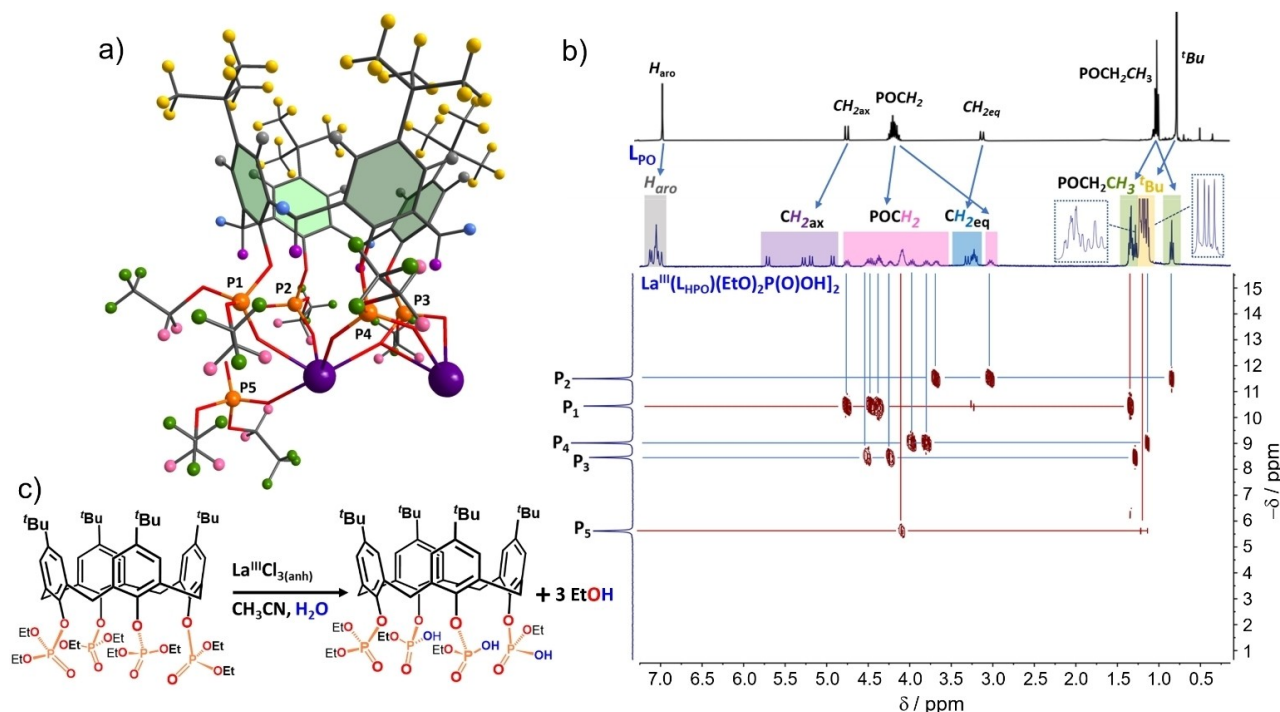

Figure 2. a) Representation of the different hydrogen atoms in **1** observable by ^1H NMR. Removal of the La atom on the right formally yields the asymmetric unit as observed by SCXRD. Color code: H–aromatics = gray, H–CH_2axial = purple, H–$POCH_2CH_3$ = pink, H–CH_2equatorial = blue, H–$POCH_2CH_3$ = green, and H–^tButyl = yellow. b) (top) ^1H NMR spectra (400 MHz, 300 K) of L_{PO} in $CDCl_3$ and (bottom) ^{31}P-^1H HMBC NMR spectrum of **1** in $CDCl_3$. c) Reaction showing the conversion of L_{PO} into H_3L_{HPO} and the release of three EtOH equivalents per L_{PO}.

Chemistry–A European Journal

Research Article
doi.org/10.1002/chem.202203525

Chemistry
Europe
European Chemical
Societies Publishing

then resonate at -9.02 ppm. Unfortunately, Nuclear Overhauser effect spectroscopy (NOESY) experiments failed in the correlation of protons close in space in the different phosphoryl units. That is not surprising when considering the disposition of these groups, pointing outwards in the molecular structure.

NMR studies on the hydrolysis of L$_{PO}$

To obtain more information on the hydrolysis reaction of L$_{PO}$ we performed ^{1}H NMR (400 MHz, CD$_3$CN) experiments at different time intervals. The initial reaction mixture corresponds to $[L_{PO}]_o = 5.75$ mM and different concentrations of La^{III}Cl$_3$ in 0.8 mL of CD$_3$CN (entries 1–4, Table 1). Results observed in reactions with entries 1–3 in Table 1 show similar behavior: a) at $t=0$ h, there are no NMR signals corresponding to the free L$_{PO}$ ligand (all of which is coordinated); b) ^{1}H/^{31}P NMR peaks at $t=0$ h presented almost identical shifts to $[Y^{III}(L_{PO})_2]^{3+}$ (Figure 1a) and the unpublished complex $[Y^{III}(L_{PO})(H_2O)_4]^{3+}$ (Figures S8, S9), supporting the presence of the lanthanum analogs; c) we observed a progressive decrease of the $[La^{III}(L_{PO})_2]Cl_3$ signals as the EtOH concentration increased (Figure 3); d) the consump-

tion of $[La^{III}(L_{PO})(H_2O)_4]Cl_3$ is only detected when the concentration of $[La^{III}(L_{PO})_2]Cl_3$ is very small, towards the end of the reaction; e) the molar intensity of EtOH is three times larger than the disappearance of $[L_{PO}]$ signals in the form of both afore-mentioned complexes. This behavior continues in the measured time and is well-described by first-order kinetics in the time interval presented in Table 1.

Surprisingly the increase of lanthanum salt in the reaction mixture decreases the rate of the reaction (entries 1–3, Table 1). The reaction with the lowest La^{III}Cl$_3$ concentration (entry 4, Table 1), contains (at $t=0$) $[La^{III}(L_{PO})_2]Cl_3$ and an unidentified complex different from $[La^{III}(L_{PO})(H_2O)_4]Cl_3$. This reaction has the highest rate constant, although it starts to saturate after 12 h to reach a final conversion of 42% (vs. 61% for entry 3, see Figure S10 and Table S4). These experiments suggest that the consumed L$_{PO}$ is present in the form of $[La^{III}(L_{PO})_2]Cl_3$ during the reaction time described in Table 1, and suggest the hydrolysis of three P–OEt bonds per L$_{PO}$ molecule. However, the experiments do not provide enough information to ascertain if the active lanthanum species is calixarene-supported or not. The presence of possible intermediates of the reactions could not be detected as the lifespan of these species are too short with respect to the NMR timescale at room temperature.

Table 1. First-order rate constants and half-life times measured for different hydrolysis reaction mixtures at 300 K and $[L_{PO}]_o = 5.75$ mM. L$_{PO}$ is in the form of a coordinated ligand. Values of K extracted from Table S4.

Entry	Reaction mixture [LaCl$_3$]/[L$_{PO}$]	Reaction time [min]	k [10^{-4} min^{-1}]	$t_{1/2}$ [10^3 min][a]
1	3	0 to 3000	1.96	3.54
2	2	0 to 2880	2.36	2.94
3	1	0 to 2160	3.61	1.92
4	0.5	0 to 720	6.94	0.99

Results are calculated by ^{1}H NMR (400 MHz, CD$_3$CN) spectroscopy using anisole as an internal standard. The H$_2$O observed in the CD$_3$CN amounts to 0.06 mmol for a 0.8 mL solution. [a] $t_{1/2} = \ln(2)/k$.
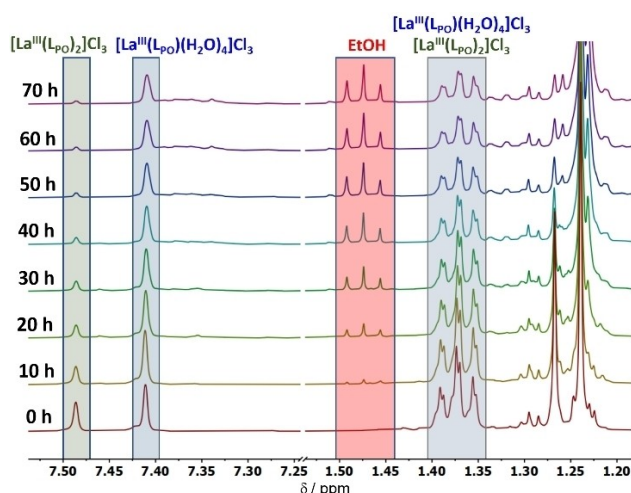

Figure 3. ^{1}H NMR (400 MHz, 300 K) spectra of a reaction mixture of 13.8×10^{-3} mmol of LaCl$_3$ and 4.6×10^{-3} mmol of L$_{PO}$ in 0.8 mL of CD$_3$CN as a function of reaction time, related to entry 1 in Table 1. Signals related to CH$_{2ax/eq}$ and methylene-POCH$_2$ are strongly mixed and difficult to interpret.

UV-Vis, FT-IR, ESI-MS and TGA experiments

The electronic absorption spectra of **1–4** in chloroform solution display an intense band at 240 nm ($\varepsilon \sim 1.8 \cdot 10^4$ M^{-1} cm^{-1}), and two moderately intense bands at 274 and 282 nm ($\varepsilon \sim 0.60 \cdot 10^4$ M^{-1} cm^{-1}), attributed to a $\pi \rightarrow \pi^*$ electronic transition centered on the phenyl rings of calixarene and phosphoryl moieties (Figure S11, right). $[Ln^{III}(L_{HPO})((EtO)_2P(O)OH)]_2$ dimers appear distinct from the neutral L$_{PO}$ ligand in terms of their electronic absorption properties; while L$_{PO}$ present broad, low-intensity absorption bands at 272 and 280 nm, **1–4** show more intense absorption bands at 274 and 282 nm, with similar features at 240 nm (Figure S11, left). FT–IR spectra of **1–4** display vibrations associated with ν(C–H) ~ 2961–2864 cm^{-1} (s), ν(arC–C) ~ 1478 cm^{-1} (s), overlapping vibrations of ν(P–OPh/P=O/C–O) ~ 1250–1100 cm^{-1} (vs), ν(P–OEt) ~ 1098–1020 cm^{-1} (vs) and ν(P(V)–O) ~ 970–940 cm^{-1} (s) (Figures S12–S14). High-resolution ESI-MS negative ion-mode data for complexes **1−4** show the presence of one main ion, the singly charged $[M+(EtO)_2P(O)O)]^-$ with a relative abundance of 100%, where M = $[Ln^{III}(L_{HPO})]_2$ (Figures S15–S18). To investigate the thermal stability, thermogravimetric decomposition experiments of complexes **1−4** were carried out in an inert atmosphere. All compounds exhibit thermal stability up to ca. 230°C, wherefrom a ~ 10% mass loss is observed up to 280°C corresponding to the loss of co-crystallized CH$_3$CN solvent molecules. A more progressive mass decrease (~ 11%) between 280 and 380°C is most likely related to the loss of the two terminal diethyl hydrogen phosphates (Figures S19, S20). Elemental analyses of **1–4** agree with the empirical formula C$_{116}$H$_{176}$O$_{40}$P$_{10}$Ln$_2$ (Ln = La, Dy, Tb, and Gd) with deviations within 0.1% (see Experimental section).

Chemistry–A European Journal

Research Article
doi.org/10.1002/chem.202203525

**Chemistry
Europe**
European Chemical
Societies Publishing

Magnetic properties

Direct current (dc) magnetic susceptibility and magnetization measurements of **2–4** are shown in Figure 4a as $\chi_m T$ versus T at 0.1 T and M_m versus B at 2 K and $B = 0.1–5.0$ T. At 290 K, the $\chi_m T$ value of 15.59 cm³ K mol⁻¹ (**4**–Gd) is within the anticipated range of 15.2–15.7 cm³ K mol⁻¹ for two non-interacting Gd^{III} centers.[14] Upon cooling, the $\chi_m T$ value remains constant up to 4 K, a typical behavior for isotropic Gd^{III} spin centers. Subsequently, the $\chi_m T$ value slightly rises to 15.87 cm³ K mol⁻¹ at 2.0 K, indicating a weak ferromagnetic exchange interaction between the Gd ions. At 2.0 K, the molar magnetization M_m value for **4** rapidly increases to 11.7 $N_A\mu_B$ at 1.5 T, wherefrom it slowly reaches 13.9 $N_A\mu_B$ at 5.0 T – close to the saturation value of two Gd^{III} centers (14 $N_A\mu_B$). The $\chi_m T$ value of the anisotropic magnetic centers in **2** and **3** at 290 K (28.09 cm³ K mol⁻¹ (**2**–Dy) and 23.67 (**3**–Tb)) are within the ranges of 26.0–28.1 and 23.5–24.0 cm³ K mol⁻¹ expected[14] for two non-interacting Dy^{III} and Tb^{III} centers, respectively. As the temperature lowers, the $\chi_m T$ value of **2** marginally increases to 28.48 cm³ K mol⁻¹ at 140 K, from which it steadily decreases to a minimum of 26.45 cm³ K mol⁻¹ at 12 K. Below this temperature there is a rapid increase to a maximum of 28.69 cm³ K mol⁻¹ at 2.0 K. For **3**, the $\chi_m T$ value continuously increases upon decreasing temperature, showing a maximum of 26.05 cm³ K mol⁻¹ at 40 K, with a subsequent decrease to 23.42 cm³ K mol⁻¹ at 2.0 K. In principle, ferromagnetic exchange interactions cause a steadily growing increase of $\chi_m T$ upon decreasing temperatures. The shape of the $\chi_m T$ vs. T curves in **2** and **3** below 100 K is determined by two opposing effects: the thermal depopulation of the m_J energy states of the ground term (in total $(2J+1)^2$ states with $J = 15/2$ (**2**) and 6 (**3**)) and the superexchange interaction between the μ-O-bridged metal centers; we note that the Zeeman effect at 0.1 T is small in comparison to these contributions. At 2.0 K, the molar magnetization rapidly increases to 9.9 (**2**) and 10.0 $N_A\mu_B$ (**3**), respectively, at 1.0 T. At higher magnetic fields, M_m continuously increases to 11.1 (**2**) and 11.5 (**3**) $N_A\mu_B$, at 5.0 T. These represent about half of the expected saturation values for two Dy^{III} ($2\times g_J J N_A\mu_B = 20$ $N_A\mu_B$, $g_J = 4/3$) and Tb^{III} (18 $N_A\mu_B$, $g_J = 3/2$) centers, in line with the magnetic anisotropy and measurement of randomly oriented crystallites of the bulk sample.

We fitted the experimental data of **4** to a Hamiltonian using an effective spin model ($\hat{S} = 7/2$), the Zeeman effect (μ_B is the Bohr magneton, B the applied magnetic field and g_{eff} the g-factor of the Gd^{III} ions) and the isotropic exchange interactions J, see Equation (1).

$$\widehat{H} = g_{eff}\,\mu_B \sum_{i=1}^{2} \boldsymbol{B} \cdot \widehat{\boldsymbol{S}}_i - 2J\,\widehat{\boldsymbol{S}}_1 \cdot \widehat{\boldsymbol{S}}_2 \qquad (1)$$

The least-squares fit with a quality of 0.5 % (relative root mean squared error) yields the parameters $g_{eff} = 1.99 \pm 0.01$, $J = +0.01 \pm 0.01$ cm⁻¹ resulting in a ground state with $S_{total} = 7$.

The ac susceptibility of compounds **2–4** in oscillating magnetic fields at zero and other static bias fields (up to 1000 Oe) revealed out-of-phase signals only for **2**. The marginal signals at zero static magnetic bias field could be enhanced by the application of a static 500 Oe field (see Figure 4) to detect out-of-phase signals up to 8.5 K. In Figure 3b–c the mixing of another relaxation pathway can be observed at temperatures lower than 3 K and high frequencies; these data were neglected in the fitting of the experimental data. We analyzed the ac features in terms of a generalized Debye expression[15] by simultaneously fitting χ_m' versus f (Figure 4b) and χ_m'' versus f (Figure S21) data at these temperatures. The calculated relaxation times τ with the distribution $\alpha = 0.157 \pm 0.069$ are plotted against the inverse temperature (Figure 4d) and suggest the presence of several relaxation pathways. The best fit to τ versus $1/T$ data is found for the combination of direct and Raman relaxation processes by using the equation $\tau^{-1} = A_K T + CT^n$. The least-squares fit yields the constant $A_K = 338 \pm 17$ s⁻¹ K⁻¹ for the direct process, and the constant $C = 0.87 \pm 0.25$ s⁻¹ K⁻ⁿ with $n = 5.5 \pm 0.2$ for the Raman process. For Kramers' ions such as Dy^{III}, an exponent of $n = 5$ corresponds to a spin-one-phonon interaction in second order for closely spaced energy levels, and an exponent of 6 corresponds to an optical acoustic Raman-like process.[16] The dominant Raman relaxation process is more likely to be the former since it is more commonly found.
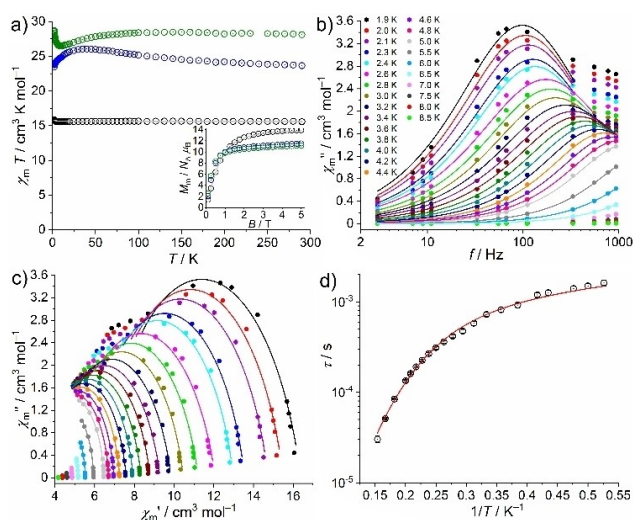

Figure 4. Magnetic dc data of **2–4**: a) $\chi_m T$ vs. temperature T at 0.1 T. Inset: molar magnetization M_m vs. magnetic field B at 2.0 K; experimental data of **2** (green), **3** (blue), and **4** (black open circles), least-squares fit of **4** data using an effective isotropic spin model (solid gray line). (b–d) Magnetic ac data of **2** at a static bias field of 500 Oe: b) Out-of-phase susceptibility χ_m'' vs. frequency f. c) Cole-Cole plot of χ_m'' vs. in-phase magnetic susceptibility χ_m' in the range 1.9–8.5 K (filled circles: data, lines: least-squares fits). d) Arrhenius plot of relaxation times τ vs. inverse temperature $1/T$ (the solid red line shows a combined fit considering a direct and a Raman relaxation processes).

Conclusion

In summary, lanthanide-based controlled hydrolysis in the phosphorylated-calix[4]arene (L_{PO}) unit turns L_{PO} into a new hydrolyzed-phosphoryl-calix[4]arene (H_3L_{HPO}) ligand. In the reaction conditions employed, the anionic and chelating nature

Chemistry–A European Journal

Research Article
doi.org/10.1002/chem.202203525

Chemistry Europe
European Chemical
Societies Publishing

of H_3L_{HPO} locks the two lanthanide metal ions in the sandwich-type $[Ln^{III}(L_{HPO})((EtO)_2P(O)OH)]_2$ complexes **1–4**, restricting further hydrolysis in the phosphoryl groups and negating the possibility of obtaining complexes with higher nuclearity. Although a very limited number of calix[4]arene scaffolds derivatized with phosphoryl ester groups also exist,[6,17] this work represents the first study targeting the hydrolysis of phosphorylated-calix[4]arene to isolate lanthanide-based calix[4]arene complexes. Investigation of the magnetic properties of **2–4** reveals slow magnetization relaxation dynamics for the Dy derivative, best reproduced when considering a combination of direct and Raman relaxation processes. Based on the observed reaction space, we conjecture that the title compounds could provide valuable/relevant information to researchers interested in the development of synthetic materials as mimics of nuclease enzymes. Current work focuses on two different routes: a) further investigations into the hydrolysis reaction of L_{PO} via lanthanide metal ions under different reaction conditions and b) the isolation of H_xL_{HPO} ligands ($x=1$–8) by using acid/base non-coordinating substrates and their subsequent coordination to lanthanide ions to understand its coordinating possibilities in the quest for new polynuclear complexes. Results stemming from the ongoing work will be communicated in due course and may lead to a better understanding of the complex formation mechanism and establish magneto-structural correlations.

Experimental Section

All reagents and solvents were used as received from commercial suppliers without further purification. The precursor tetrakis-O-(diethoxyphosphoryl)-p-tert-butylcalix[4]arene (L_{PO}) was prepared according to a literature procedure.[4b] Additional information regarding instrumentation; ESI-HRMS, UV-Vis, IR, TGA and PXRD data; magnetic studies and crystallographic analysis details are given in the Supporting Information.

Synthesis of $[Ln^{III}(L_{HPO})((EtO)_2P(O)OH)]_2$

$Ln^{III}Cl_3$ (0.10 mmol), L_{PO} (0.1193 g, 0.10 mmol) and $(EtO)_2P(O)ONa$ (0.0528 g, 0.30 mmol) were dissolved in CH_3CN and stirred for two hours. After filtration, Et_2O was diffused into the mother liquor, affording crystals of the **1–4** complexes after two weeks. Yield (0.2041 g, 73% for **1**); (0.2104 g, 74% for **2**); (0.1985 g, 70% for **3**) and (0.2096 g, 74% for **4**).

Analytical details of 1–4

$[La^{III}(L_{HPO})((EtO)_2P(O)OH)]_2$ (1)

¹H NMR (400 MHz, $CDCl_3$): δ 7.13–6.99 (m, 16H, ArH), 5.71, 5.28, 5.19, 4.93 (d, $^2J_{HH}=12.0$ Hz, 8H, CH_{2ax}), 4.74–3.68 (m, 26H, POCH_2CH_3), 3.33–3.22 (m, 8H, CH_{2eq}), 3.01 (m, 2H, POCH_2CH_3), 1.37–1.25 (m, 36H, POCH$_2$CH_3), 1.23 (s, 18H, ^{t}Bu-CH_3), 1.19 (s, 18H, ^{t}Bu-CH_3), 1.17 (s, 18H, ^{t}Bu-CH_3), 1.14 (s, 18H, ^{t}Bu-CH_3), 0.85 (t, $^2J_{HH}=7.2$ Hz, 6H, POCH$_2$CH_3) ppm; **³¹P NMR** (162 MHz, $CDCl_3$): δ −5.62, −8.46, −9.02, −10.44, −11.50 ppm. **ESI⁻ HRMS**, m/z: found 2642.6697 [M + (EtO)$_2$P(O)O]⁻ (100%), calculated for $[C_{112}H_{164}O_{36}P_9La_2]^-$: 2642.6802. M=$[La^{III}(L_{HPO})]_2$. **UV-Vis**, solution in

$CHCl_3$, λ/nm (ε/10⁴ M⁻¹ cm⁻¹): 240 (1.671), 272 (0.500), 280 (0.491). **IR**, KBr disk, ν/cm⁻¹: 2961 (m), 1478 (m), 1362 (w), 1250 (m), 1204 (s), 1158 (m), 1075 (s), 1050 (s), 1037 (s), 988 (m), 965 (m), 940 (s), 881 (m), 788 (s), 755 (m), 659 (s). **Elemental analysis**, calculated for $C_{116}H_{176}O_{40}P_{10}La_2$: C 49.79, H 6.34%. Found: C 49.82, H 6.31%. **Crystal data for 1**: $C_{116}H_{176}O_{40}P_{10}La_2$·5.5 CH_3CN, $M_r=$ 3023.87 g mol⁻¹, colorless block, 0.07×0.09×0.13 mm³, triclinic, space group P-1, $a=15.540(3)$ Å, $b=15.875(3)$, $c=16.576(3)$, $\alpha=73.72(3)°$, $\beta=77.80(3)°$, $\gamma=69.83(3)°$, $V=3654.8(16)$ Å³, $Z=1$, STOE STADIVARI diffractometer, MoKα radiation (λ= 0.71073 Å), $T=100(2)$ K, 65206 reflections collected, 13375 unique ($R_{int}=0.0938$), 9586 observed ($I>2\sigma(I)$). Final $GooF=0.988$, $R1=0.0638$ ($I>2\sigma(I)$) and $wR2=0.1516$ (all data).

$[Dy^{III}(L_{HPO})((EtO)_2P(O)OH)]_2$ (2)

ESI⁻ HRMS, m/z: found 2689.7097 [M + (EtO)$_2$P(O)O]⁻ (100%), calculated for $[C_{112}H_{164}O_{36}P_9Dy_2]^-$: 2689.7237. M=$[Dy^{III}(L_{HPO})]_2$. **UV-Vis**, solution in $CHCl_3$, λ/nm (ε/10⁴ M⁻¹ cm⁻¹): 240 (1.853), 274 (0.605), 282 (0.584). **IR**, KBr disk, ν / cm⁻¹: 2960 (m), 1478 (m), 1362 (w), 1250 (m), 1213 (s), 1164 (m), 1104 (s), 1078 (s), 1053 (s), 990 (m), 941 (s), 881 (m), 795 (s), 756 (m), 686 (w), 661 (m), 592 (m), 502 (s). **Elemental analysis**, calculated for $C_{116}H_{176}O_{40}P_{10}Dy_2$: C 48.97, H 6.23%. Found: C 49.02, H 6.37%. **Crystal data for 2**: $C_{116}H_{176}O_{40}P_{10}Dy_2$·5 CH_3CN, $M_r=3050.53$ g mol⁻¹, colorless block, 0.125 x 0.30 x 0.31 mm³, triclinic, space group P-1, $a=15.560(3)$ Å, $b=15.956(3)$, $c=16.271(3)$ Å, $\alpha=74.04(3)°$, $\beta=79.09(3)°$, $\gamma=70.53(3)°$, $V=3617.2(15)$ Å³, $Z=1$, STOE STADIVARI diffractometer, MoKα radiation (λ= 0.71073 Å), $T=100(2)$ K, 84725 reflections collected, 13706 unique ($R_{int}=0.110$), 11781 observed ($I>2\sigma(I)$). Final $GooF=1.051$, $R1=0.0594$ ($I>2\sigma(I)$) and $wR2=0.1634$ (all data).

$[Tb^{III}(L_{HPO})((EtO)_2P(O)OH)]_2$ (3)

ESI⁻ HRMS, m/z: found 2682.7121 [M + (EtO)$_2$P(O)O]⁻ (100%), calculated for $[C_{112}H_{164}O_{36}P_9Tb_2]^-$: 2682.7189. M=$[Tb^{III}(L_{HPO})]_2$. **UV-Vis**, solution in $CHCl_3$, λ/nm (ε/10⁴ M⁻¹ cm⁻¹): 240 (1.783), 274 (0.601), 282 (0.587). **IR**, KBr disk, ν / cm⁻¹: 2960 (m), 1478 (m), 1392 (w), 1362 (w), 1299 (w), 1249 (w), 1211 (s), 1163 (m), 1101 (s), 1078 (s), 1053 (s), 990 (m), 967 (m), 941 (s), 881 (m), 795 (m), 756 (m), 686 (m), 661 (m), 592 (m), 500 (m). **Elemental analysis**, calculated for $C_{116}H_{176}O_{40}P_{10}Tb_2$: C 49.09, H 6.25%. Found: C 49.12, H 6.20%. **Crystal data for 3**: $C_{116}H_{176}O_{40}P_{10}Tb_2$·5.5 CH_3CN, $M_r=$ 3063.89 g mol⁻¹, colorless block, 0.140 x 0.150 x 0.330 mm³, triclinic, space group P-1, $a=15.454(3)$ Å, $b=15.955(3)$, $c=16.266(3)$, $\alpha=74.10(3)°$, $\beta=79.03(3)°$, $\gamma=70.54(3)°$, $V=3615.3(15)$ Å³, $Z=1$, STOE STADIVARI diffractometer, MoKα radiation (λ= 0.71073 Å), $T=100(2)$ K, 75870 reflections collected, 13245 unique ($R_{int}=0.0314$), 12288 observed ($I>2\sigma(I)$). Final $GooF=1.065$, $R1=0.0353$ ($I>2\sigma(I)$) and $wR2=0.0954$ (all data).

$[Gd^{III}(L_{HPO})((EtO)_2P(O)OH)]_2$ (4)

ESI⁻ HRMS, m/z: found 2679.7078 [M + (EtO)$_2$P(O)O]⁻ (100%), calculated for $[C_{112}H_{164}O_{36}P_9Gd_2]^-$: 2679.7168. M=$[Gd^{III}(L_{HPO})]_2$. **UV-Vis**, solution in $CHCl_3$, λ/nm (ε/10⁴ M⁻¹ cm⁻¹): 240 (1.762), 274 (0.623), 282 (0.610). **IR**, KBr disk, ν / cm⁻¹: 2960 (m), 1478 (m), 1390 (w), 1362 (w), 1299 (w), 1211 (s), 1163 (m), 1101 (s), 1078 (s), 1051 (s), 967 (m), 941 (s), 881 (m), 788 (s), 755 (m), 661 (m), 592 (m), 500 (m). **Elemental analysis**, calculated for $C_{116}H_{176}O_{40}P_{10}Gd_2$: C 49.15, H 6.26%. Found: C 49.22, H 6.36%. Only the unit cell was measured: triclinic, space group P-1, $a=15.552(8)$ Å, $b=15.857(9)$, $c=16.579(6)$ Å, $\alpha=73.91(4)°$, $\beta=77.87(3)°$, $\gamma=69.75(4)°$, $V=$

Chemistry–A European Journal

Research Article
doi.org/10.1002/chem.202203525

Chemistry Europe
European Chemical
Societies Publishing

Acknowledgements

Conflict of Interest

The authors declare no conflict of interest.

Data Availability Statement

The data that support the findings of this study are available from the corresponding author upon reasonable request.

[1] a) C. D. Gutsche, in *Calixarenes: An Introduction*, 2nd ed., The Royal Society of Chemistry, Cambridge, 2008, ch. 2, pp. 27–160; b) C. R. Driscoll, B. L. Reid, M. J. McIldowie, S. Muzzioli, G. L. Nealon, B. W. Skelton, S. Stagni, D. H. Brown, M. Massi, M. I. Ogden, *Chem. Commun.* 2011, *47*, 3876–3878; c) G. Karotsis, S. Kennedy, S. J. Teat, C. M. Beavers, D. A. Fowler, J. J. Morales, M. Evangelisti, S. J. Dalgarno, E. K. Brechin, *J. Am. Chem. Soc.* 2010, *132*, 12983–12990; d) P. D. Beer, M. G. B. Drew, A. Grieve, M. Kan, P. B. Leeson, G. Nicholson, M. I. Ogden, G. Williams, *Chem. Commun.* 1996, 1117–1118; e) M. Massi, M. I. Ogden, *Materials* 2017, *10*, 1369; f) G. Karotsis, S. J. Teat, W. Wernsdorfer, S. Piligkos, S. J. Dalgarno, E. K. Brechin, *Angew. Chem. Int. Ed.* 2009, *48*, 8285–8288; *Angew. Chem.* 2009, *121*, 8435–8438; g) P. K. Thallapally, B. P. McGrail, S. J. Dalgarno, H. T. Schaef, J. Tian, J. L. Atwood, *Nat. Mater.* 2008, *7*, 146–150; h) J. L. Atwood, L. J. Barbour, S. J. Dalgarno, M. J. Hardie, C. L. Raston, H. R. Webb, *J. Am. Chem. Soc.* 2004, *126*, 13170–13171.

[2] a) D. N. Woodruff, R. E. P. Winpenny, R. A. Layfield, *Chem. Rev.* 2013, *113*, 5110–5148; b) A. Gaita-Ariño, F. Luis, S. Hill, E. Coronado, *Nat. Chem.* 2019, *11*, 301–309; c) E. Moreno-Pineda, C. Godfrin, F. Balestro, W. Wernsdorfer, M. Ruben, *Chem. Soc. Rev.* 2018, *47*, 501–513; d) A. Ghirri, A. Candini, M. Affronte, *Magnetochemistry* 2017, *3*, 12; e) S. Thiele, F. Balestro, R. Ballou, S. Klyatskaya, M. Ruben, W. Wernsdorfer, *Science* 2014, *344*, 1135–1138; f) G. Aromí, D. Aguilà, P. Gamez, F. Luis, O. Roubeau, *Chem. Soc. Rev.* 2012, *41*, 537–546; g) A. Cornia, M. Mannini, P. Sainctavit, R. Sessoli, *Chem. Soc. Rev.* 2011, *40*, 3076–3091; h) M. Urdampilleta, N. V. Nguyen, J. P. Cleuziou, S. Klyatskaya, M. Ruben, W. Wernsdorfer, *Int. J. Mol. Sci.* 2011, *12*, 6656–6667; i) L. Bogani, W. Wernsdorfer, *Nat. Mater.* 2008, *7*, 179–186.

[3] a) L. R. B. Wilson, M. Coletta, M. Evangelisti, S. Piligkos, S. J. Dalgarno, E. K. Brechin, *Dalton Trans.* 2022, *51*, 4213–4226; b) R. McLellan, M. A. Palacios, S. Sanz, E. K. Brechin, S. J. Dalgarno, *Inorg. Chem.* 2017, *56*, 10044–10053; c) M. Coletta, R. McLellan, A. Waddington, S. Sanz, K. J. Gagnon, S. J. Teat, E. K. Brechin, S. J. Dalgarno, *Chem. Commun.* 2016, *52*, 14246–14249; d) M. A. Palacios, R. McLellan, C. M. Beavers, S. J. Teat, H. Weihe, S. Piligkos, S. J. Dalgarno, E. K. Brechin, *Chem. Eur. J.* 2015, *21*, 11212–11218; e) S. Sanz, R. D. McIntosh, C. M. Beavers, S. J. Teat, M. Evangelisti, E. K. Brechin, S. J. Dalgarno, *Chem. Commun.* 2012, *48*, 1449–1451; f) S. Sanz, K. Ferreira, R. D. McIntosh, S. J. Dalgarno, E. K. Brechin, *Chem. Commun.* 2011, *47*, 9042–9044.

[4] a) F. Gao, L. Cui, Y. Song, Y. Z. Li, J. L. Zuo, *Inorg. Chem.* 2013, *53*, 562–567; b) M. Hosseinzadeh, S. Sanz, J. V. Leusen, N. V. Izarova, E. K. Brechin, S. J. Dalgarno, P. Kögerler, *Chem. Commun.* 2021, *57*, 8087–8090; c) Y. Jiao, S. Sarwar, S. Sanz, J. van Leusen, N. V. Izarova, C. L. Campbell, E. K. Brechin, S. J. Dalgarno, P. Kögerler, *Dalton Trans.* 2021, *50*, 9648–9654.

[5] W. Kläui, *Angew. Chem. Int. Ed. Engl.* 1990, *29*, 627–637.

[6] J. M. Harrowfield, M. Mocerino, B. J. Peachey, B. W. Skelton, A. H. White, *J. Chem. Soc. Dalton Trans.* 1996, 1687–1699.

[7] a) L. M. Zimmermann, G. I. Almerindo, J. R. Mora, I. H. Bechtold, H. D. Fiedler, F. Nome, *J. Phys. Chem. C* 2013, *117*, 26097–26105; b) B. Gamoke, D. Neff, J. Simons, *J. Phys. Chem. A* 2009, *113*, 5677–5684; c) S. E. Hosseini, H. Saeidian, A. Amozadeh, M. T. Naseri, M. Babri, *Rapid Commun. Mass Spectrom.* 2016, *30*, 2585–2593.

[8] a) S. C. L. Kamerlin, P. K. Sharma, R. B. Prasad, A. Warshel, *Q. Rev. Biophys.* 2013, *46*, 1–132; b) W. W. Cleland, A. C. Hengge, *Chem. Rev.* 2006, *106*, 3252–3278; c) S. K. Silverman, *Acc. Chem. Res.* 2015, *48*, 1369–1379; d) L. Jiang, Y. Sun, Y. Chen, P. Nan, *ChemistrySelect* 2020, *5*, 9492–9516.

[9] J. A. Cowan, *Chem. Rev.* 1998, *98*, 1067–1088.

[10] J. M. Berg, J. L. Tymoczko, G. J. Gatto Jr., L. Stryer, *Biochemistry*, 9th ed., New York, NY: W. H. Freeman and Co., 2019.

[11] Y. Lan, S. Gai, K. Cheng, F. Yang, *Environ. Sci. Water Res. Technol.* 2022, *8*, 1173–1187.

[12] a) N. Sträter, W. N. Lipscomb, T. Klabunde, B. Krebs, *Angew. Chem. Int. Ed.* 1996, *35*, 2024–2055; *Angew. Chem.* 1996, *108*, 2158–2191; b) G. Schenk, N. Mitić, G. Hanson, P. Comba, *Coord. Chem. Rev.* 2013, *257*, 473–482; c) N. Mitić, S. J. Smith, A. Neves, L. W. Guddat, L. R. Gahan, G. Schenk, *Chem. Rev.* 2006, *106*, 3338–3363; d) P. V. Bernhardt, S. Bosch, P. Comba, L. R. Gahan, G. R. Hanson, V. Mereacre, C. J. Noble, A. K. Powell, G. Schenk, H. Wadepohl, *Inorg. Chem.* 2015, *54*, 7249–7263.

[13] a) J. R. Morrow, L. A. Buttrey, V. M. Shelton, K. A. Berback, *J. Am. Chem. Soc.* 1992, *114*, 1903–1905; b) B. F. Baker, H. Khalili, N. Wei, J. R. Morrow, *J. Am. Chem. Soc.* 1997, *119*, 8749–8755; c) D. M. Epstein, L. L. Chappell, H. Khalili, R. M. Supkowski, W. D. Horrocks, J. R. Morrow, *Inorg. Chem.* 2000, *39*, 2130–2134; d) K. Nwe, C. M. Andolina, J. R. Morrow, *J. Am. Chem. Soc.* 2008, *130*, 14861–14871; e) C.-H. Huang, J. Hammell, S. J. Ratnakar, A. D. Sherry, J. R. Morrow, *Inorg. Chem.* 2010, *49*, 5963–5970; f) T. L. M. Martinon, V. C. Pierre, *J. Asian J.* 2022, *17*, e2022004.

[14] H. Lueken, *Magnetochemie*, Teubner Verlag, Stuttgart, 1999.

[15] K. S. Cole, R. H. Cole, *J. Chem. Phys.* 1941, *9*, 341–351.

[16] K. N. Shrivastava, *Phys. Stat. Sol. B* 1983, *117*, 437–458.

[17] a) P. Thuery, M. Nierlich, R. Abidi, Z. Asfari, J. Vicens, *Z. Kristallogr. NCS* 1999, *214*, 154–156; b) J. Lipkowski, M. Vysotski, J. Slowikowska, V. I. Kalchenko, L. N. Markovsky, *J. Phys. Org. Chem.* 1998, *11*, 63–70; c) L. N. Markovsky, M. A. Visotsky, V. V. Pirozhenko, V. I. Kalchenko, J. Lipkowski, Y. A. Simonov, *Chem. Commun.* 1996, 69–71; d) J. Gloede, I. Keitel, B. Costisella, A. Kunath, M. Schneider, *Phosphorous, Sulfur, and Silicon* 1996, *117*, 67–88; e) J. Gloede, B. Costisella, M. Ramm, R. Bienert, *Phosphorous, Sulfur, and Silicon* 1993, *84*, 217–222.